STRUCTURAL CHEMISTRY

ISSN 2053-2296

# Role of weak C—H···O and strong N—H···O intermolecular interactions on the high-symmetry molecular packing of *trans*-cyclohexane-1,4-dicarboxamide

Fernando García-Reyes,[a] Adolfo C. Fantoni,[a] Máximo Barón,[b] Rosana M. Romano,[c] Graciela M. Punte[a] and Gustavo A. Echeverría[a,d]*

[a]IFLP (CONICET, CCT–La Plata) – Departamento de Física, Facultad de Ciencias Exactas, Universidad Nacional de La Plata, 115 y 49, 1900 La Plata, Argentina, [b]Facultad de Ciencias Exactas y Naturales, Universidad de Belgrano, Villanueva 1324, 1426 Buenos Aires, Argentina, [c]CEQUINOR (UNLP–CONICET, CCT–La Plata), Departamento de Química, Facultad de Ciencias Exactas, Universidad Nacional de La Plata, 1900 La Plata, Argentina, and [d]Facultad de Ingeniería, Universidad Nacional de La Plata, 115 y 49, 1900 La Plata, Argentina. *Correspondence e-mail: geche@fisica.unlp.edu.ar

Received 7 June 2018
Accepted 20 August 2018

Edited by N. Lugan, Laboratoire de Chimie de Coordination du CNRS, Toulouse, France

**Keywords:** crystal structure; *ab initio* calculations; hydrogen bonds; carboxamide; IR spectroscopy; Raman spectroscopy.

**CCDC reference**: 1586317

**Supporting information**: this article has supporting information at journals.iucr.org/c

An unpredicted fourfold screw N—H···O hydrogen bond $C(4)$ motif in a primary dicarboxamide (*trans*-cyclohexane-1,4-dicarboxamide, $C_8H_{14}N_2O_2$) was investigated by single-crystal X-ray diffraction and IR and Raman spectroscopies. Electron-density topology and intermolecular energy analyses determined from *ab initio* calculations were employed to examine the influence of weak C—H···O hydrogen-bond interactions on the peculiar arrangement of molecules in the tetragonal $P4_32_12$ space group. In addition, the way in which the co-operative effects of those weak bonds might modify their relative influence on molecular packing was estimated from cluster calculations. Based on the results, a structural model is proposed which helps to rationalize the unusual fourfold screw molecular arrangement.

## 1. Introduction

Understanding the role and nature of weak intermolecular interactions (noncovalent interactions) in the packing and supramolecular organization of organic molecules has been the subject of numerous and recurrent investigations and controversies since the original work of van der Waals (Van der Waals, 1873). Studies in this area helped in the establishment of the crystal engineering and supramolecular chemistry fields, which have been boosted in the last decade by interest in gaining a better understanding of biological systems and improving the performance of medicines. The historical development of these fields has been guided by the identification of extended and recurrent patterns of interactions in organic crystal structures and between organic fragments in organometallic compounds. The outcome of those efforts has been the detection of different fragments whose presence in molecules favours the formation of patterns; these fragments have been called molecular synthons (Desiraju, 1995). In spite of the awareness of the influence of noncovalent interactions in molecular recognition and aggregation, and the use of molecular synthons in diverse supramolecular synthesis, it is still a challenge to predict crystal structures from a knowledge of molecular structure (Desiraju, 1995). Strong hydrogen bonds (like O—H···O and N—H···O) are important driving forces in many synthons which have been successfully employed in crystal engineering. However, their use in supra-

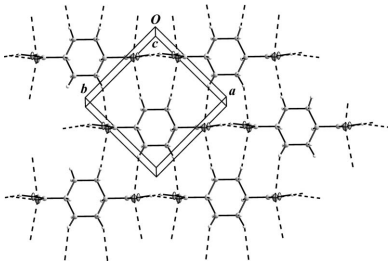

molecular synthesis depends on their robustness and transferability to different environments. Therefore, the study of these synthons when fragments favouring weak interactions, like C—H···O, are also present is a field of continuing interest. Many efforts have been dedicated to carboxamide groups not only as building blocks from which diverse structures could be assembled, but also due to their intrinsic interest as part of pharmaceutical drugs. In particular, carboxamide is a group having both strong donor and acceptor H atoms (Berkovitch-Yellin & Leiserowitz, 1980) (see Scheme 1) and depending of the residue characteristics (atom constituents, size, shape and accessible surface) will aggregate forming different homosynthons.

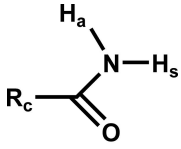

$R_C$ = residue
a = antiplanar
s = synplanar

Scheme 1

The packing modes of primary carboxamides have been extensively analyzed by Leiserowitz and several co-authors (Leiserowitz & Schmidt, 1969; Leiserowitz & Hagler, 1983) in terms of the ideal amide contacts and symmetry-packing requirements (see Fig. 1).

Combination of arrays **I** and **II** or **III** develops characteristic structural motifs. The mentioned authors have performed a comprehensive analysis and classification of the possible packing types of those motifs in mono- and diamide systems. They also found that in the case of symmetric diamide molecules, infinite chains of $R_2^2(8)$ motifs along the main molecular axis might be built. This kind of chain (Fig. 2) will be hereafter called an infinite molecular chain (IMC).

According to Leiserowitz & Hagler (1983), IMCs related by a translation or a twofold screw axis build two-dimensional (2D) layers, while those connected by a glide plane develop a steep, or shallow, structural motif. Since the IMCs forming these structural motifs are connected by N—$H_a$···O hydrogen bonds (where $H_a$ is an antiplanar carboxamide H atom), they should pack at a distance of 5.1 Å when linked by a translation axis or at a distance of about 4.9 Å if they are linked by a twofold screw axis or a glide plane.

Kuduva *et al.* (2001) have added to the findings of Leiserowitz & Hagler (1983) with a detailed examination of the modifications that weak noncovalent bonds, residue substituents and size may promote. They found that unexpected kinds of molecular packing can be induced by those factors in primary carboxamides. Within this scenario our interest in the present work is to go deeper in the rationalization of how not only residue composition or size, but also residue morphology and weak contacts involving C—H···O hydrogen bond may affect the geometry of carboxamide synthons favouring unforeseen arrangements, like the observed $4_3$ axis in compound **1** (Fig. 3 and Scheme 2).

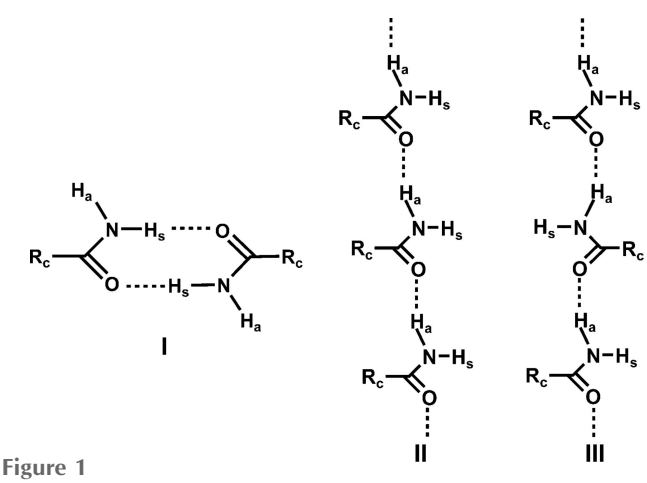

Figure 1
The array types: **I** is an $R_2^2(8)$ cyclic dimer, **II** is a translation axis and **III** is a glide plane or twofold screw axis.

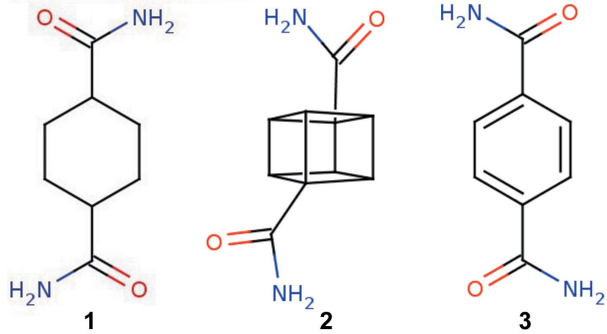

Scheme 2

With this aim and within a study of the factors that govern the molecular conformation and aggregation of *trans*-1,4-substituted cyclohexanes (Echeverría *et al.*, 1995*a*,*b*, 2000, 2003), the crystal structure of *trans*-cyclohexane-1,4-dicarboxamide, **1**, was determined by single-crystal X-ray diffraction methods and its IR and Raman spectra were recorded and analyzed. In order to ascertain the role of weak C—H···O hydrogen bonds, their nature and possible co-operative effects

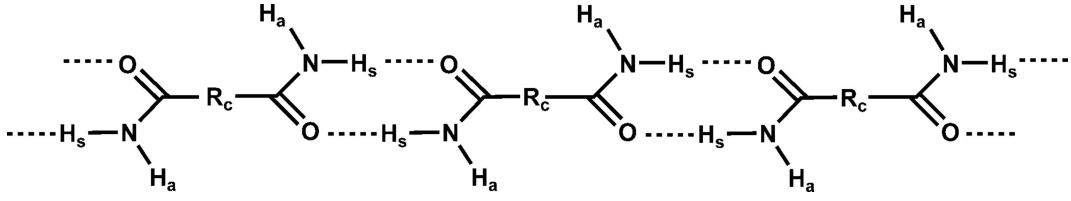

Figure 2
The infinite molecular chain (IMC).

**Table 1**
Experimental details.

| | |
|---|---|
| Crystal data | |
| Chemical formula | $C_8H_{14}N_2O_2$ |
| $M_r$ | 170.21 |
| Crystal system, space group | Tetragonal, $P4_32_12$ |
| Temperature (K) | 293 |
| $a$, $c$ (Å) | 6.9584 (2), 18.8979 (6) |
| $V$ (Å$^3$) | 915.02 (6) |
| $Z$ | 4 |
| Radiation type | Cu $K\alpha$ |
| $\mu$ (mm$^{-1}$) | 0.74 |
| Crystal size (mm) | 0.25 × 0.12 × 0.12 |
| Data collection | |
| Diffractometer | Agilent Xcalibur Eos Gemini |
| Absorption correction | Multi-scan (*CrysAlis PRO*; Agilent, 2014) |
| $T_{min}$, $T_{max}$ | 0.893, 1 |
| No. of measured, independent and observed [$I > 2\sigma(I)$] reflections | 1745, 890, 837 |
| $R_{int}$ | 0.014 |
| (sin $\theta/\lambda)_{max}$ (Å$^{-1}$) | 0.617 |
| Refinement | |
| $R[F^2 > 2\sigma(F^2)]$, $wR(F^2)$, $S$ | 0.044, 0.130, 1.07 |
| No. of reflections | 890 |
| No. of parameters | 68 |
| H-atom treatment | Only H-atom displacement parameters refined |
| $\Delta\rho_{max}$, $\Delta\rho_{min}$ (e Å$^{-3}$) | 0.23, −0.13 |
| Absolute structure | Flack $x$ determined using 278 quotients $[(I^+) - (I^-)]/[(I^+) + (I^-)]$ (Parsons *et al.*, 2013) |
| Absolute structure parameter | −0.1 (3) |

Computer programs: *CrysAlis PRO* (Agilent, 2014), *SHELXT* (Sheldrick, 2015*a*), *SHELXL2014* (Sheldrick, 2015*b*), *ORTEP-3 for Windows* (Farrugia, 1997), *Mercury* (Macrae *et al.*, 2008), and *PLATON* (Spek, 2009) and *PARST* (Nardelli, 1995) within *WinGX* (Farrugia, 2012).

in the generation of the high-symmetry structure observed in **1**, *ab initio* calculations of the molecular electron charge density and its Laplacian topology, in-crystal, in-clusters and in-gas phase geometries were performed. Orbital population changes and their contribution to intermolecular interaction energies were determined from natural bond orbital (NBO) analysis. In addition, they were calculated at different levels of theory and with different basis functions. To reinforce the conclusions, some of the results were compared with those obtained from the crystal structure analysis and calculations performed on cubane-1,4-dicarboxamide, **2**, studied by Kuduva *et al.* (2001). The results are presented and discussed below.

## 2. Experimental

### 2.1. Synthesis and crystallization

The title compound, **1**, was synthesized according to Barón *et al.* (1975). The product was crystallized by slow evaporation from acetone.

### 2.2. X-ray diffraction

H atoms were localized from difference Fourier maps and refined riding on their bound atoms. Crystal data, data collection and structure refinement details are summarized in Table 1.

### 2.3. IR and Raman spectroscopy

The FT–IR spectra were recorded on a Nexus Nicolet instrument equipped with either an MCTB or a DTGS detector (for the ranges 4000–400 and 600–50 cm$^{-1}$, respectively) at room temperature and with resolutions of 1 and 4 cm$^{-1}$. The solid compound was measured in KBr (range 4000–400 cm$^{-1}$) and polyethylene (range 600–50 cm$^{-1}$) pellets. The Raman spectra were recorded using an Horiba–Jobin–Yvon T64000 Raman spectrometer, with a confocal microscope and CCD detection, employing an excitation

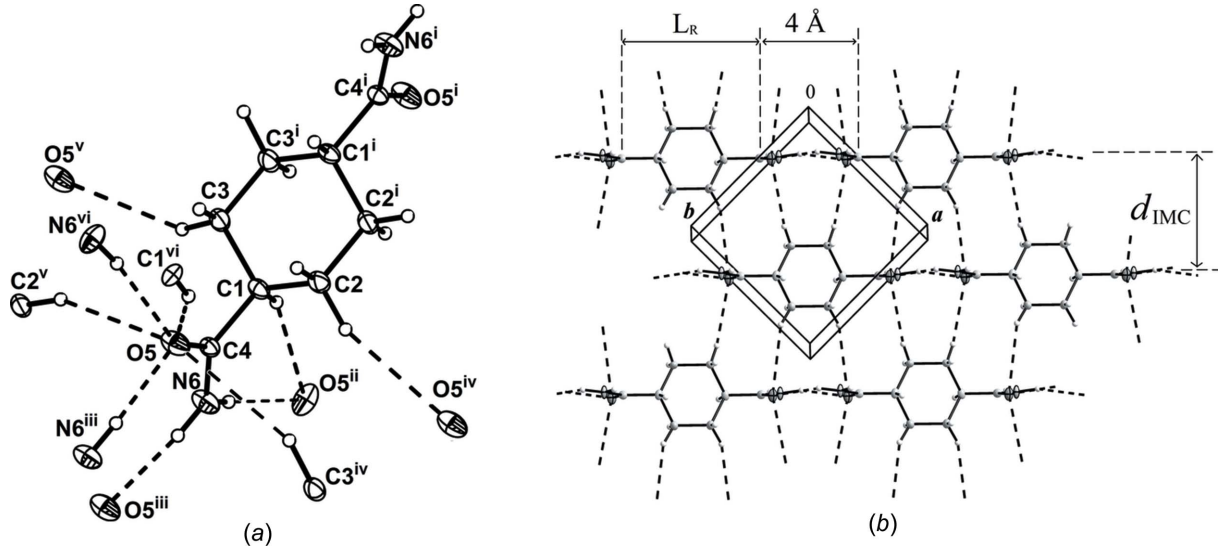


**Figure 3**
View of *trans*-cyclohexane-1,4-dicarboxamide, showing (*a*) the labelling of the non-H atoms and their displacement ellipsoids at the 30% probability level and (*b*) the *ab* layer, (001) plane, of the crystal. Hydrogen bonds are indicated by dashed lines. [Symmetry codes: (i) $y, x, -z+1$; (ii) $-y+\frac{3}{2}, x+\frac{1}{2}, z-\frac{1}{4}$; (iii) $y-1, x+1, -z+1$; (iv) $y, x+1, -z+1$; (v) $y-1, x, -z+1$; (vi) $y-\frac{1}{2}, -x+\frac{3}{2}, z+\frac{1}{4}$]. $L_R$ is the residue length and $d_{IMC}$ is the interchain distance.

Table 2
Geometries of selected intermolecular interactions calculated from fully optimized dimers at the PBE/6-31G** theory level.

X-ray difraction data are given in square brackets[a].

| Contact | Compound | H···O (Å) | $X$—H···O (°) | H···O═C (°) | $X$···O (Å) | N—C—O···H (°) |
|---|---|---|---|---|---|---|
| N—$H_s$···O | **1** | 1.8091 [1.878] | 176.47 [174.2] | 120.05 [122.8] | 2.8377 [2.890 (3)] | −1.29 [5.9] |
| | **2** | 1.7999 [1.907 (1)] | 176.06 [164.0] | 119.62 [118.8] | 2.8290 [2.897 (2)] | 0.00 [18.4] |
| N—$H_a$···O | **1** | 1.9230 [1.956] | 175.98 [167.5] | 137.49 [135.0] | 2.9378 [2.955 (3)] | −164.96 [−137.8] |
| | **2** | 1.9501 [1.935] | 167.70 [154.8] | 131.32 [126.5] | 2.9551 [2.886 (2)] | 160.58 [−138.3 (1)] |
| C—$H_{in}$···O | **1** | 2.8655 [2.504] | 140.67 [150.1] | 121.90 [138.2] | 3.7803 [3.492 (3)] | 130.32 [140.2] |
| | **2** | 2.5068 [2.654] | 146.42 [144.8] | 115.00 [129.5] | 3.4678 [3.599 (3)] | 123.58 [−146.8] |
| C—$H_{out}$···O | **1** | 2.4895 [2.795/2.982] | 148.80 [155.3/150.1] | 109.22 [87.1/81.4] | 3.4730 [3.811 (4)/3.957 (4)] | 85.15 [−81.8/78.3] |
| | **2** | 2.2870 [2.612] | 177.59 [154.5] | 125.24 [93.4] | 3.3769 [3.625 (2)] | 87.27 [86.1] |

Note: (*a*) H-atom positions are corrected after normalizing $X$—H bond lengths to neutron diffraction standard values. $H_{out}$ and $H_{in}$ denote H atoms bonded to residue C atoms lying perpendicular and parallel to the carboxamide plane, respectively.

wavelength of 514.5 nm from an Ar multiline laser. The wavenumbers were calibrated with the 459 $cm^{-1}$ band of $CCl_4$.

### 2.4. *Ab initio* calculations

Molecular orbital calculations in molecules and supramolecular arrangements, as well as the corresponding NBO analysis, were performed using *GAUSSIAN03* (Frisch *et al.*, 2004). Electron-density topology analysis and the topology of the negative Laplacian of a charge-density examination, based on the quantum theory of atoms in molecules (QTAIM; Bader, 1990), were performed using the AIM2000 code (Biegler-König & Schönbohm, 2002). All geometry optimizations were undertaken at the PBE/6-31G** level of theory, except for the IR and Raman spectral calculations, where the MP2/6-311++G(d,p) theory level was employed. In all the optimizations, the experimental geometry was utilized as the starting point.

Calculations of NBO, electron charge density topologies and intermolecular interaction energies for each intermolecular interaction were performed at the MP2 and PBE/aug-cc-pVDZ theory levels. For the intermolecular interaction energies, the supermolecule and counterpoise methods, which account for the basis set superposition error (BSSE), were employed (Boys & Bernardi, 1970; Simon *et al.*, 1996).

Periodic calculations were performed with *CRYSTAL14* (Dovesi *et al.*, 2014) on the X-ray-determined geometry, with H-atom positions corrected after normalizing the $X$—H bond lengths to neutron diffraction standard values. The B3LYP hybrid method, in combination with the standard 6-31G** basis set, was used, keeping shrinking factors and convergence thresholds at their default values. An AIM topological analysis of the resulting electron density was performed using *TOPOND14* (Gatti & Casassa, 2014).

## 3. X-ray results

Compound **1** crystallizes in the noncentrosymmetric tetragonal $P4_32_12$ space group. The molecules are located on a twofold symmetry axis with half a molecule in the asymmetric unit. As observed in other symmetrical *trans*-1,4-di- and tetrasubstituted cyclohexanes, the molecules adopt a rigid chair conformation. The –$CONH_2$ groups are equatorially bonded to the six-membered ring C atoms, with the –$CONH_2$ group rotated by 86.1 (1)° out of the mean molecular plane. In accordance with expectations, the carboxamide groups account for the main intermolecular interactions. As shown in Fig. 3, the molecules are involved in strong N—H···O hydrogen bonds linking the carboxamide groups and in weak

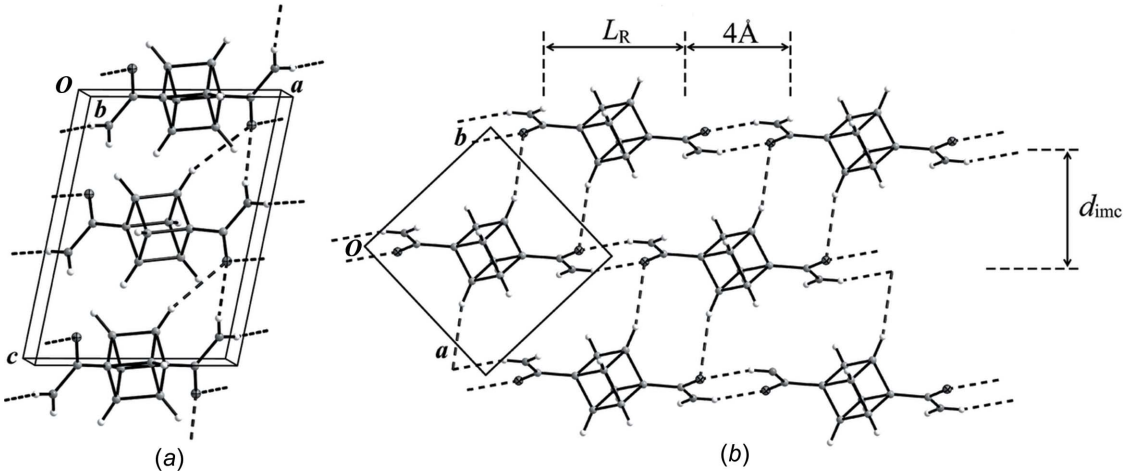


Figure 4
View of (*a*) the unit cell along *b* and (*b*) the *ab* layer along the [001] direction of compound **2**. Intermolecular interactions between carboxamide groups (*i.e.* N—H···O contacts) and between these groups and residues (*i.e.* C—H···O contacts) are shown as dashed lines.

**Table 3**
Values of the most relevant topological parameters of intermolecular (3,−1) charge density CPs, evaluated at the PBE/6-31G** theory level for clusters **I** and **II**[a].

The subscripts $x$ = a or s indicate antiplanar or synplanar carboxamide H atoms and $y$ = in or out represent C—H groups oriented in or out of the carboxamide plane.

| Contacts | Compound | $\rho(r)$ (e A$^{-3}$) | $\nabla^2\rho(r)$ (e A$^{-5}$) | $\lambda_3$ (e A$^{-5}$) |
|---|---|---|---|---|
| N—H$_s$···O | **1** | 0.2247 | 2.2884 | 4.5124 |
| | **2** | 0.2314 | 2.4308 | 4.7490 |
| N—H$_a$···O | **1** | 0.1566 | 1.7486 | 3.1217 |
| | **2** | 0.1718 | 1.8356 | 3.3832 |
| C—H$_{in}$···O | **1** | 0.0469 | 0.5597 | 0.8408 |
| | **2** | 0.0803 | 0.8597 | 1.4336 |
| C—H$_{out}$···O | **1** | 0.0453 | 0.5792 | 0.8289 |
| | **2** | 0.0455 | 0.5647 | 0.8433 |

Note: (*a*) $\rho(r)$ electron density, its Laplacian, $\nabla^2\rho(r)$, and positive principal curvature, $\lambda_3$, evaluated at the corresponding (3,−1) critical points.

C—H···O hydrogen bonds connecting ring C atoms and carbonyl O atoms. Relevant geometric information is listed in Table 2.

Carboxamide groups, related by a twofold axis, build characteristic $R_2^2(8)$ homosynthons, *i.e.* **I** (Fig. 1), forming twofold symmetry IMCs (Fig. 2). The IMCs run along the [110] and [$\bar{1}$10] crystallographic directions (Fig. 3). Along the [001] direction (Fig. 3*a*), IMCs are related by N—H$_a$···O hydrogen bonds. Consecutive IMCs are arranged perpendicular to each other, forming a $C(4)$ motif with an unusual fourfold screw symmetry. The structure is further stabilized in this direction by a weaker C—H$_{ax}$···O hydrogen bond linking the H atom axially (ax) bonded to the substituted ring C atom to the carbonyl O atom. Additionally, within the *ab* layer (Fig. 3*b*), the IMCs are also connected by C—H$_{eq}$···O contacts between H atoms equatorially (eq) bonded to unsubstituted ring C atoms and carbonyl O atoms. Similar weak C—H···O hydrogen-bond interactions have been observed previously in monosubstituted cyclohexanecarboxamide by Zipp *et al.* (2009) and in cubane-1,4-dicarboxamide, **2,** by Kuduva *et al.* (2001). It should be noted that in all the mentioned C—H···O contacts, the H atom bonded to an unsubstituted C atom approaches to the carbonyl O atoms nearly perpendicular to the $R_2^2(8)$ cyclic dimer plane (for details, see Table 2), pointing to the $\pi$(C═O) bond, instead of the expected approach to the

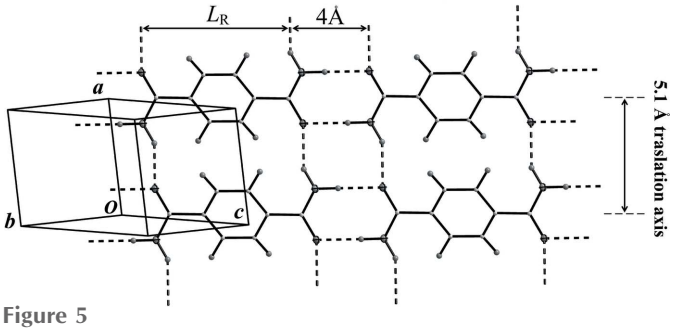


**Figure 5**
A view of the (011) layer of compound **3**. Intermolecular interactions between carboxamide groups (*i.e.* N—H···O contacts) are shown as dashed lines. Residue C—H···O contacts within this layer are absent.

$sp^2$ O-atom lone pairs. This finding might be explained on the same grounds as those employed by Gatti *et al.* (1994) to account for the four hydrogen bonds involving the carbonyl O atoms in urea.

To investigate the possible causes of the unpredicted fourfold screw axes in the molecular packing of a primary carboxamide, the packing of **1** was compared with those of cubane-1,4-dicarboxamide (**2**) [Cambridge Structural Database (Groom *et al.*, 2016) refcode HIDTET (Kuduva *et al.*, 2001)] and terephthalamide (**3**) (Cobbledick & Small, 1972; Takamizawa & Miyamoto, 2014; refcode TRPHAM) (see Scheme 2). Compound **2** crystallizes in the $P2_1/c$ space group with the carboxamide groups assembled in the shallow motif, while **3** crystallizes in the $P\bar{1}$ space group with the carboxamide groups arranged in characteristic 2D hydrogen-bond ribbon motifs, both described by Leiserowitz (1976) (Figs. 4 and 5). Following Leiserowitz & Hagler (1983), we will define residue length ($L_R$) as the intramolecular distance between carboxamide C atoms along the molecular axis (*i.e.* the line connecting the carboxamide C atoms) (Figs. 3, 4 and 5). The longest cross sectional dimension of the residue ($D_R$) of these systems are similar in the three compounds, *i.e.* 5.4 < $D_R$ < 5.8 Å, while the smallest cross sectional dimensions ($d_R$) are different; the value increases when going from terephthalamide **3** (3.4 Å) through cyclohexanecarboxamide **1** (4.9 Å) to cubanedicarboxamide **2** (5.4 Å). Thus, a comparative study of the molecular packing of the three compounds might help to shed light on the influence of geometric residue differences, which affect the spatial arrangement of the C—H groups, on the resulting three-dimensional (3D) array.

In spite of the significant symmetry differences between compounds **1** and **2**, the cross sections of the residues (*i.e.* $D_R$ and $d_R$) in both compounds are close to or even larger than the carboxamide translation of 5.1 Å. According to previous discussion and literature findings (Leiserowitz & Hagler, 1983; Kuduva *et al.*, 2001), those values favour the IMC to be assembled with their axes making an angle between them, as parallel IMC patterns will result in unfavourable H···H residue contacts.

In contrast, in compound **3**, although $D_R$ is also larger than 5.1 Å, the IMCs are packed forming the characteristic parallel ribbon pattern. This could be rationalized taking into account that its $d_R$ is 3.4 << 5.1 Å and a ring plane rotation ($\alpha$) out of the IMC layer (or carboxamide plane) larger than 20° (cos$\alpha$ < 5.1 Å axis/$D_R$) must reduce the effective residue size along the carboxamide plane promoting the ribbon motif. Actually, the measured angle is 24.4 (1)° (Cobbledick & Small, 1972; Leiserowitz, 1976) (Fig. 5).

In **2**, according to Leiserowitz & Hagler (1983), the IMCs forming the shallow-glide motif are packed along the *c* axis through N—H$_a$···O hydrogen bonds, with the carboxamide C atom close to the glide plane (*bc* layer) to fulfill the geometric requirement on the N—H$_a$···O hydrogen bond. The centrosymmetric IMCs lie parallel, on a plane perpendicular to the packing direction (*i.e.* the *ab* layer, see Fig. 4*b*), hereinafter called CL layers. From the Leiserowitz condition, the estimated distance between IMCs ($d_{IMC}$, see Fig. 4*b*) within these

Table 4
Intermolecular energies calculated at the MP2 and HF/aug-cc-pVDZ theory levels using the supermolecule and NBODel methods for dimers **I**, **II** and **III** optimized at the PBE/6-31G** theory level[a].

| Cluster | Contacts | $N^b$ | Compound | $\Delta E$ (kcal mol$^{-1}$) | | |
|---|---|---|---|---|---|---|
| | | | | $E_{MP2}$ | $E_{HF}$ | $E_{NBO}{}^c$ |
| **I** | N—$H_s$···O | 2 | **1** | −7.3 | −5.9 | −21.3 |
| | | 2 | **2** | −7.5 | −6.2 | −22.2 |
| **II** | N—$H_a$···O/ C—$H_{in}$···O | 2/2 | **1** | −10.1 | −4.9 | −14.6 |
| | | 2/2 | **2** | −10.9 | −4.7 | −16.1 |
| **III** | C—$H_{out}$···O | 4 | **1** | −1.8 | 0.0 | −3.0 |
| | | 2 | **2** | −2.2 | −0.8 | −5.7 |

Notes: (*a*) intermolecular hydrogen bonds are labelled as N—$H_x$···O and C—$H_y$···O, where subscript $x$ = a or s for antiplanar or synplanar carboxamide H atoms and $y$ = in or out for C—H groups oriented in or out of the carboxamide plane. (*b*) The number of hydrogen bonds per molecule. (*c*) Calculated as the dimer energy variation when the interacting orbitals are deleted, see text for further details.

layers is 4.8322 Å (Leiserowitz & Hagler, 1983), which is close to the measured $d_{IMC}$ distance of 4.880 (2) Å (Kuduva *et al.*, 2001). These values are larger than 4.4 Å, half the sum of the van der Waals radii of the carboxamide group (3.4 Å), and the largest molecular cross section $D_R$ (5.4 Å), suggesting that the distance between parallel IMCs is mainly determined by the packing of CLs through N—$H_a$···O and not C—H···O hydrogen bonds acting within these layers (*i.e.* C···O and H···O distances obtained from X-ray data are larger than those from *ab initio* calculations; see Table 2 and the text below for further details).

In **1**, in order that the IMCs can pack through a $4_3$-fold screw axis by N—$H_a$···O hydrogen bonds, the carboxamide C atoms should be located near the fourfold screw axis. As a result, the estimated *c* cell parameter should be around 19.6 Å, close to the experimental value of 18.8979 (6) Å. Translation of this motif along the *a* and *b* cell parameters generates a 3D structure that can be described by the tetragonal $P4_3$ space group. As in the glide motif, in the $4_3$ motif, the IMCs are perpendicular to the $4_3$ axis, forming layers of parallel IMCs.

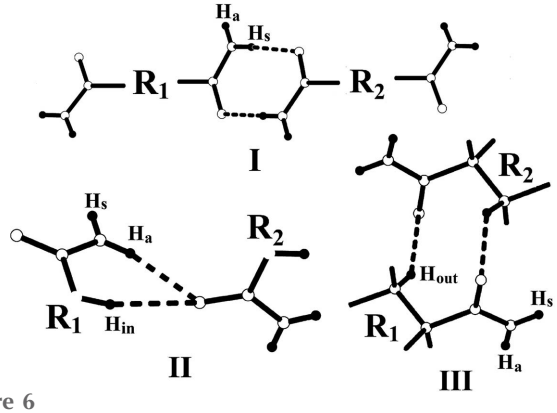


Figure 6
The three types of selected dimers and their contact labels. R is the residue in compounds **1** or **2**. $H_{out}$ and $H_{in}$ are the H atoms outside and within the carboxamide plane. In **II**, R-substituted C atoms are not drawn as $H_{in}$ may be bound to a substituted **1** or an unsubstituted **2** C atom. In **III**, not depicted terminal atoms in covalent bonds may be either H or unsubstituted C atoms. Besides, only one C—H···O hydrogen bond is observed in **2**.

These CL layers are stabilized by C—$H_{eq}$···O hydrogen bonds. Furthermore, as the molecules are located on a twofold axis, the IMCs should exhibit the same symmetry. The twofold axes are perpendicular to the $4_3$ axis and form a 3D structure of $P4_32_12$ symmetry. In this space group, all the $4_3$ axes are symmetrically equivalent and the distance between them should be 4.9 Å (cell parameter *a* is 6.9 Å), a value determined by the average size between the $R_2^2(8)$ cyclic dimer (∼4 Å) and the residue ($L_R$ ∼ 5.8 Å). These values are in excellent agreement with the measured $d_{IMC}$ distances in the CL layer of 4.9203 (2) Å or the experimental *a* cell parameter of 6.9584 (2) Å. As in **2**, in **1**, the $d_{IMC}$ distance is larger than 4.6 Å, half the sum of the van der Waals radii of the carboxamide group (3.4 Å) and the largest molecular cross section $D_R$ (5.8 Å), and close to the 4.9 Å distances calculated as ($L_R$ + 4)/2. Therefore, it could be concluded that, as in **2**, the $d_{IMC}$ values are determined mainly by the CL packing through the N—$H_a$···O hydrogen bond and not by the weak C—$H_{eq}$···O hydrogen bonds operating within these layers.

As discussed above, parallel IMCs should interact mainly through weak intermolecular C—H···O interactions. However, in **1** and **2**, morphological differences between the residues causes the C—H groups to be arranged in a peculiar way. Despite the $d_{IMC}$ distance being determined by N—$H_a$···O hydrogen bonds, weak contacts might affect the approach of the IMCs in both compounds. Thereby, influencing some critical structural parameters which are relevant in the packing of CLs (in our case, as will be seen in the discussion section, it is the tilt angle of the carboxamide plane out of the corresponding CL). But, before going into this point, it is worth evaluating the attractive and co-operative nature of selected intermolecular hydrogen bonds.

## 4. Theoretical calculations

### 4.1. Energy and charge density analysis

Energy and charge density analysis were performed for the dimers depicted in Fig. 6, using their fully optimized geometries (see §2.4).

Calculated hydrogen-bond geometries for **1** and **2** are reported in Table 2. The values of the most relevant topological parameters of the electron charge densities calculated at each intermolecular critical point [$\rho(r_c)$, $\nabla^2\rho(r_c)$ and $\lambda_3$] for compounds **1** and **2** are listed in Table 3. Other topological charge density parameters are included in the supporting information.

Hereafter C—H groups bonded to residue C atoms will be labelled as C—$H_{in}$ and C—$H_{out}$ according to their orientation relative to the carboxamide plane.

The theoretical and experimental geometries of the N—$H_s$···O and N—$H_a$···O hydrogen bonds in **1** and **2** are very similar. In contrast, a noticeable deviation of the calculated geometries from the experimental ones is observed in the weak C—$H_{out}$···O hydrogen bonds, where the calculated C···O distances are smaller than the experimental ones, supporting the attractive character of these contacts.

**Table 5**
Electron acceptor and donor orbital population change.

| Overlapping orbitals | $\Delta n_{donor}$ (e)[a] | $\Delta n_{acceptor}$ (e)[a] |
|---|---|---|
| | Dimer **I** | |
| $n(O)\rightarrow\sigma^*(H_s-N)$ | −0.03 | 0.03 |
| | Dimer **II** | |
| $n(O)\rightarrow\sigma^*(H_a-N)/\sigma^*(H_{in}-C)$ | −0.017 | 0.016/0.000[b] |
| | Dimer **III** | |
| $\pi(C{=}O)\rightarrow\sigma^*(H_{out}-C)$[c] | −0.002 | 0.002 |

Notes: (*a*) population variations when interacting orbitals are deleted. (*b*) As explained in the text, in the optimized geometry of dimer **II**, the H···O distance is too long to alter significantly the population of the $\sigma^*(H_{in}$–C) antibonding orbital, but in the crystal geometry it changes by about 0.002 e. (*c*) Optimized in the $C_i$ point group.

**Table 6**
Co-operative contribution to the interaction energy as a function of the cluster size, calculated at the MP2/6-31G(d,p) theory level.

The calculated values at the PBE/6-31G(d,p) theory level are given in parentheses.

| Cluster series | Hydrogen bonds | Cluster size | |
|---|---|---|---|
| | | Trimer | Tetramer |
| **I** | $N-H_s\cdots O$ | −0.05 (−0.04) | −0.10 (−0.11) |
| **II** | $N-H_a\cdots O + C-H_{in}\cdots O$ | −1.02 (−0.92) | −2.40 (−2.42) |
| **III** | $C-H_{out}\cdots O$ | 0.2 (0.3) | 0.6 (1.1) |

Conversely, the calculated C—O distances in the $C-H_{in}\cdots O$ contact is larger than the experimental value. This behaviour can be rationalized considering that the equilibrium state of dimer **II** is reached from the competition of two hydrogen bonds, *i.e.* strong $N-H_a\cdots O$ and weak $C-H_{in}\cdots O$. Hence, the strong bond prevails over the weak one.

The QTAIM electron charge density analysis of all selected hydrogen bonds shows (3,−1) critical points, compatible with the existence of a bond path between the H atoms of the N—H and C—H groups and the carbonyl O atom, endorsing the attractive nature of these intermolecular interactions. As is shown in Table 3, the positive $\nabla^2\rho(r_c)$ and $\lambda_3$ values in all the hydrogen bonds are characteristic of the closed-shell nature of the intermolecular interactions. As expected, the charge density evaluated at critical points, $\rho(r_c)$, in $C-H_{in}\cdots O$ and $C-H_{out}\cdots O$ hydrogen bonds are much smaller than those in the $N-H_a\cdots O$ and $N-H_s\cdots O$ hydrogen bonds, indicating that weak interactions contribute with very little energy to the crystal packing.

To better understand the characteristics of the intermolecular interactions, mainly those of the carbonyl-group intermolecular interactions, the negative Laplacian ($-\nabla^2\rho$) charge density topology around the carbonyl O atom (in the VSCC or valence shell charge concentration) was calculated for the free molecule and the bulk using the experimental geometries of **1** and **2**. The results show for the carbonyl plane, as found by Gatti *et al.* (1994) in urea, two equivalent (3,−3) CPs with average values of 147.1 and 138.6 e Å$^{-5}$ in **1**, and 147.4 and 138.2 e Å$^{-5}$ in **2** for the free molecule and the crystal state, respectively. These nonbonded maxima (NBM) can be associated with the O$sp^2$ electron lone pairs. Furthermore, in the VSCC O atoms there are two additional (3,−1) CPs with average values of 95.2 and 87.5 e Å$^{-5}$ at mean C═O···CP angles of 179.6 and 132.6° in **1**, and of 94.1 and 88.5 e Å$^{-5}$ at C═O···CP angles of 179.4 and 129.2° in **2** for the free molecule and the crystal state, respectively. These CPs are saddle points (SP) interconnecting the NBMs and along the line connecting these (3,−1) CPs with the O atom they behave like maxima of electron charge density. Contrary to the observation of the free molecules in the crystal phase, they are located out of the carbonyl plane. All these electron rich regions around the carbonyl O atoms are aligned with charge depletion near the H atoms along the N—H and C—H bonds. Therefore, it could be concluded that, during the molecular packing process, the electron charge density around the O atom is altered in a manner that increases its ability to act as a proton acceptor, being involved not only with proton-donor groups pointing towards the $sp^2$ lone-pair lobes, but also with those pointing to the $\pi$(C═O) bond.

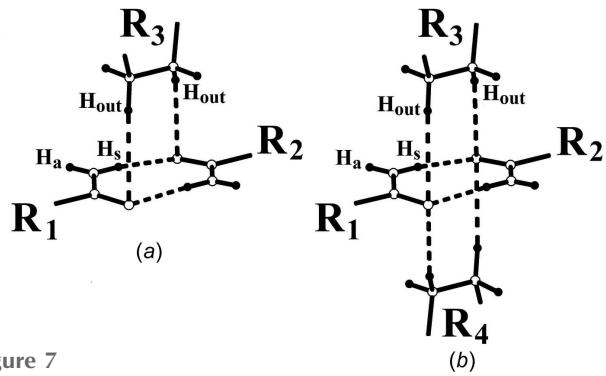


**Figure 7**
The relevant portion of the molecules in (*a*) a trimer and (*b*) a tetramer built from dimer **III**. *trans*-Cyclohexane-1,4-dicarboxamide molecules are labelled with $R_i$ ($i$ = 1, ..., 4).

The energies of the N—H···O and C—H···O hydrogen bonds are listed in Table 4, where subscript $x$ = a or s for antiplanar or synplanar carboxamide H atoms and $y$ = in or out for C—H groups oriented in or out of the carboxamide plane. They were obtained from the intermolecular energies calculated at the MP2/aug-cc-pVDZ theory level, using the supermolecule method in dimers **I**, **II** and **III** (see Fig. 6), and the counterpoise procedure (Boys & Bernardi, 1970), which considers the BSSE. The $N-H_x\cdots O$ hydrogen-bond energies are four or five times greater than those of the $C-H_y\cdots O$ hydrogen bonds, in agreement with our results from X-ray structure and charge density analysis. Despite the N···O in-crystal or dimer-optimized distance of the $N-H_a\cdots O$ hydrogen bond being larger than that of the $N-H_s\cdots O$ hydrogen bond (see Table 2), its energy is bigger by about 3 kcal mol$^{-1}$ (1 kcal mol$^{-1}$ = 4.184 kJ mol$^{-1}$). This suggests that weak hydrogen bonds of the C—H···O type, such as $C-H_{in}\cdots O$, may contribute to the stabilization energy of dimer **II**. A mixture of both hydrogen bonds is included in Table 4, together with the hydrogen-bond energies calculated at the HF/aug-cc-pVDZ theory level. A comparison of the $E_{MP2}$ and $E_{HF}$ energies for the studied hydrogen bonds shows that the largest variation is observed in weak $C-H_{out}/H_{in}\cdots O$ hydrogen bonds, thus indicating a significantly dispersive character for these interactions.

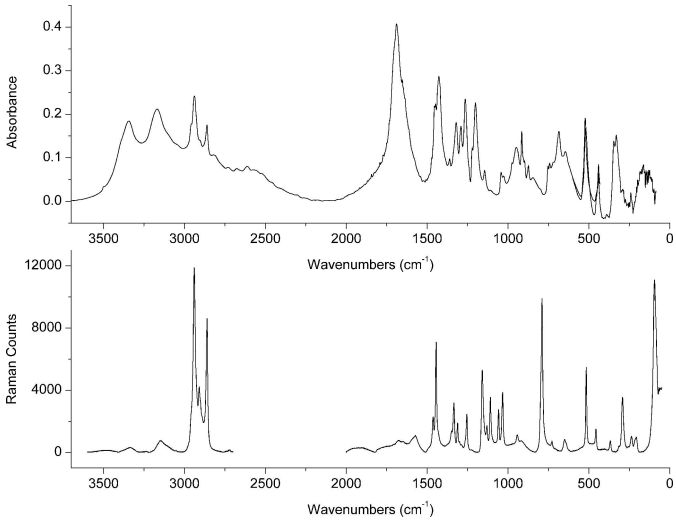


**Figure 8**
FT–IR (top, ranges 3700–400 and 600–80 $cm^{-1}$) and Raman (bottom, ranges 3600–2700 and 2000–50 $cm^{-1}$) spectra of solid *trans*-cyclohexane-1,4-dicarboxamide, **1**.

### 4.2. NBO analysis

The NBO method was also employed to delve deeper into the nature of the intermolecular interactions of compound **1**. The results will allow us not only to characterize the orbitals involved in the interactions but also their contribution to the stabilization energy. As stated by Reed & Weinhold (1986), a small amount of charge transfer between these orbitals could contribute significantly to the intermolecular energy. In the optimized dimers **I**, **II** and **III** (see Fig. 6), the interaction energy, $E_{NBO}$, and population change, $\Delta n$, of the interacting natural orbitals were evaluated from the NBO deletion method as implemented in *GAUSSIAN03* (Frisch *et al.*, 2004) (all elements in the Fock matrix between interacting atoms of both fragments were deleted, and the resulting matrix was rediagonalized). All NBO calculations were performed at the PBE/aug-cc-pVDZ theory level. A summary of the electron-donor and -acceptor orbitals involved in the hydrogen bonds is given in Table 5, while their associated contributions to the stabilization energies are listed in Table 4. These results indicate the charge-transfer contribution to the N—$H_x\cdots$O hydrogen bonds from the overlapping carbonyl O-atom electron lone pairs $n$(O) (from the mixing of the *s* and *p* oxygen natural atomic orbitals) to the unoccupied $\sigma^*$(N—$H_x$) antibonding orbitals of the amide group, resulting in an interaction of the $n$(O)→$\sigma^*$($H_x$—N) type.

In contrast, the charge transfer in weak C—$H_{out}\cdots$O (C—$H_{eq}\cdots$O) hydrogen bonds between unsubstituted cyclohexane C and carbonyl O atoms results from the overlapping of the carbonyl $\pi$(C═O) bond orbital with the $\sigma^*$(C—$H_{out}$) antibonding orbital of the unsubstituted cyclohexane C atoms. Hence, this interaction can be described as the $\pi$(C═O)→$\sigma^*$($H_{out}$—C) type. The change in the electron population of the interacting orbitals is a measure of the charge transfer between them and is proportional to the stabilization energy of the intervening species (Reed & Weinhold, 1986). The NBO occupation number of the electron lone pairs of carbonyl group, *i.e.* $n$(O), decreased by 0.030 e in dimer **I** and 0.017 e in dimer **II**. In contrast, the antibonding orbital $\sigma^*$(N—$H_s$) in **I** and $\sigma^*$(N—$H_a$) in **II** increase by a similar amount, *i.e.* 0.031 and 0.016 e, respectively, with respect to the population orbitals evaluated when the associated NBO Fock matrix elements are deleted. On the other hand, using the same procedure, the population of the NBO $\pi$(C═O) bond orbital in dimer **III** decreases by a value of 0.002 e, while the occupation number of the interacting $\sigma^*$($H_{out}$—C) antibonding orbital increases by about 0.002 e. The last values are about an order of magnitude smaller than those of $n$(O) and the $\sigma^*$($H_s$—N) and $\sigma^*$($H_a$—N) orbitals. This suggests that the contribution of the interaction energy due to the charge transfer between occupied and unoccupied orbitals in strong N—$H_x\cdots$O hydrogen bonds should be significantly greater than those in weak C—$H_y\cdots$O hydrogen bonds (Table 3). Furthermore, a comparison of the $E_{MP2}$ and $E_{NBO}$ values for each contact, listed in Table 4, shows that in strong N—$H_x\cdots$O hydrogen bonds, the absolute value of $E_{MP2}$ is smaller than $E_{NBO}$, showing that the charge transfer contribution to the stabilization energy could be significant in these contacts. On the other hand, in weak C—$H_y\cdots$O hydrogen bonds, the behaviour is less pronounced, indicating a more electrostatic character.

### 4.3. Analysis of the co-operative effect

Charge transfer might influence the co-operative effect in hydrogen bonds (Hongwei *et al.*, 2005), mainly when interactive fragments have groups with delocalized electrons. As a consequence, it could be inferred that the N—$H_a\cdots$O, N—$H_s\cdots$O, C—$H_{out}\cdots$O and C—$H_{in}\cdots$O hydrogen-bond interactions observed in **1** and **2** could contribute differently to the co-operative effect depending on whether they connect fragments involving delocalized or localized electrons. Thus, in order to study in compound **1** the different co-operative contributions of each interaction to the intermolecular energy, three series of clusters were built. The first and second series are built from dimers **I** [*i.e.* from the $R_2^2(8)$ cyclic dimer] and **II** for chains of increasing length up to tetramers. These series of clusters allow us to study the contributions of the N—$H_a\cdots$O, N—$H_s\cdots$O and C—$H_{in}\cdots$O hydrogen bonds to the co-operative effect. On the other hand, the contribution of the C—$H_{out}\cdots$O hydrogen bonds to the co-operative effect are studied by comparing the trimer and tetramer built from dimer **III** in Fig. 6 by adding a third and fourth molecule as is shown in Fig. 7.

The intermolecular interaction energy of a given cluster was evaluated as the cluster energy minus the energy of each monomer (for $i$, an integer, running over all molecules in the cluster, $N$) evaluated in the cluster basis set for the BSSE.

$$E_{int} = E_{cluster} - \sum_{i=1}^{N} E_i.$$

The co-operative effect could be understood as the deviation of the total interaction energy of the cluster from the sum of the interaction energies between each molecule pairs ($E_{ij}$),

such a deviation being just the total many-body contribution to the total interaction energy. That is

$$E_{\rm coop} = E_{\rm int} - \sum_{ij=1}^{N} E_{ij}$$

where the $E_{ij}$ terms are calculated in the cluster basis set.

In Table 6 are listed the contributions of the co-operative effect to the intermolecular interaction energy as a function of the cluster size. The co-operative contribution of the N—$H_a$···O hydrogen bond is larger than in N—$H_s$···O. Although the N—$H_a$···O hydrogen bond could be assisted by charge delocalization within the $R_2^2(8)$ cyclic dimer ring known as RAHB (resonance-assisted hydrogen bond) according to Gilli *et al.* (1989), its co-operative contribution does not significantly increase with the cluster size. In contrast, the N—$H_a$···O hydrogen bonds have a significantly increase with cluster enlargement due to the contribution of the co-operative effect. These results could be rationalized as being due to the confinement of RAHB and charge-transfer effects to the $R_2^2(8)$ cyclic dimers in clusters **I**, while the charge delocalization is extended over the entire infinite $C(4)$ chain in cluster **II**. Furthermore, although the co-operative effect of the weak C—$H_{out}$ ···O hydrogen bond only adds a small amount of energy, its contribution might be destabilizing (Table 6).

## 5. IR and Raman results

The IR and Raman spectra of **1** are shown in Fig. 8. The vibrational analysis was performed comparing experimental IR and Raman spectra with those reported in the literature, as well as with those obtained by calculations at the MP2 level with the 6-311++G(d,p) basis set from optimized molecular geometry, at the same level, for the isolated molecule. To avoid the anharmonic effects and limitations of calculations (Jensen, 2007) which induce calculated frequency values larger than the experimental ones, the calculated frequencies were corrected by the factor 0.9483 proposed by Scott & Radom (1996). The inclusion of this factor allows us to have more realistic calculated frequencies and a better agreement between the calculated and experimental values.

Although the molecule strictly has no symmetry centre, the deviation from a centrosymmetric structure is only very small. This is reflected in the relative intensities of the bands in the IR and Raman spectra. The molecule presents 72 normal vibrational modes, most of them active either in the IR or in the Raman spectra. A complete list of the experimental IR and Raman wavenumbers, together with the calculated frequencies and tentative assignments, is presented as supporting information (Table S2).

The molecule presents four vibrational modes associated with the two $NH_2$ groups. Two of them, assigned to $\nu_{as}(NH_2)$(in-phase) and $\nu_s(NH_2)$(out-of-phase) modes, are IR active and were observed at 3345 and 3170 $cm^{-1}$, respectively, as broad absorptions in the solid FT–IR spectrum. A comparison of these two absorptions with the calculated frequencies for the isolated molecule, predicted at 3560 and 3424 $cm^{-1}$, reveals that these wavenumbers are red-shifted in the IR spectrum of the solid, showing that they are involved in strong N—H···O=C hydrogen-bond interactions. The Raman spectrum presents two low-intensity bands in this spectral region assigned to the other two vibrational modes, *i.e.* $\nu_{as}(NH_2)$(out-of-phase) and $\nu_s(NH_2)$(in-phase), at approximately 3336 and 3147 $cm^{-1}$, respectively. Eight $\nu(CH_2)$ modes are observed between 2958 and 2901 $cm^{-1}$, four of them in the IR spectrum and the other four in the Raman spectrum, in coincidence with the results of the calculations, which predict these vibrations in the 2966–2902 $cm^{-1}$ range. The $\nu$(CH) in-phase (Raman active) and out-of-phase (IR active) modes of the substituted C atoms of the ring appeared around 2860 $cm^{-1}$, while the calculated frequencies are 2894 and 2893 $cm^{-1}$, respectively. These values are about 30 $cm^{-1}$ higher than those found experimentally and could be considered as evidence that the associated bands are red-shifted.

The band at 1689 $cm^{-1}$ and its shoulder at 1644 $cm^{-1}$ in the FT–IR spectrum can be assigned to the out-of-phase C=O

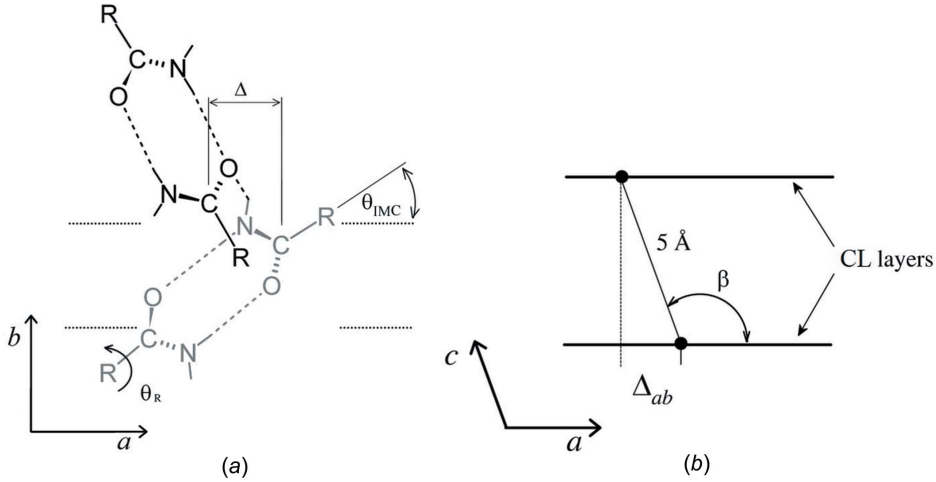


**Figure 9**
(*a*) A projection perpendicular to the *ab* layer of two linked carboxamide $R_2^2(8)$ cyclic dimers through the N—$H_a$···O contact. The $R_2^2(8)$ cyclic dimer in a molecular plane is shown in grey behind that in black. (*b*) A projection down the *b* axis showing the parallel Δ shift between CL layers.

stretching and $NH_2$ scissoring modes, respectively. The in-phase modes are observed in the Raman spectrum at 1678 and 1647 $cm^{-1}$. As presented in Table S2 of the supporting information, the $NH_2$ scissoring modes are clearly blue-shifted (approximately 100 $cm^{-1}$) with respect to the expected values for the isolated molecules. The calculated frequency values are 1679 $cm^{-1}$ for both C═O stretching modes and 1546/1545 $cm^{-1}$ for the in-phase/out-of-phase $NH_2$ scissoring modes. When amide groups are involved in strong interactions, the wavenumbers of the $NH_2$ scissoring bands usually increase with the strength of the N—H···O═C hydrogen bond (Lin-Vien *et al.*, 1991), thus decreasing the difference between their values with respect to the C═O stretching bands. Thus, the IR and Raman spectra of the solid present clear evidence of strong hydrogen-bond interactions. The rest of the bands in the FT–IR and Raman spectra are fully consistent with the theoretically simulated spectra, as can be observed in Table S2 of the supporting information.

## 6. Discussion

As described above, in **1**, each $H_{out}$ atom (equatorial $H_{eq}$ atom) establishes four similar intermolecular C—$H_{out}$···O contacts to carboxamide O atoms of two adjacent IMCs (see Table 2). The sum of the calculated intermolecular energies provided by those contacts to the stabilization energy is −7.2 kcal $mol^{-1}$ (Table 4). Therefore, it is comparable to that supplied by the N—$H_a$···O and C—$H_{in}$···O (or C—$H_{ax}$···O) hydrogen bonds, *i.e.* −10.1 kcal $mol^{-1}$, to the stabilization energy. It appears that weak C—$H_{out}$ ···O interactions acting in concert may well stabilize the carboxamide plane perpendicular to the CL layer (see Fig. 3*b*).

On the other hand, in **2**, assuming the molecular conformation does not deviate from that of the gas phase during crystallization, there are two possible orientations of the molecular chains that leave the carboxamide groups approximately perpendicular to the CL layer (*ab* layer). In one of them, the cubyl C—$H_{out}$ groups are pointing, perpendicular to the double N—$H_s$···O hydrogen-bonded ring plane (cyclic dimer **I**), to the amide N atoms of neighbouring parallel IMCs, building four C—$H_{out}$···N contacts. In the other arrangement of chains (rotated 180° from the previous one around the chain axis), the cubyl C—$H_{out}$ groups are pointing, perpendicular to the double N—$H_s$···O hydrogen-bonded ring plane, to O atoms of adjacent parallel IMCs. In this way, they build four C—$H_{out}$ ···O contacts, as in **1**, instead of four C—$H_{out}$···N contacts. An estimation of how much contribution to the inter-chain energy would furnish C—$H_{out}$···N and C—$H_{out}$···O hydrogen bonds in both ideal IMCs arrangements were obtained at the PBE/aug-cc-pDVZ theory level by building suitable geometry optimized cluster models. The C—$H_{out}$ ···N hydrogen bond contributes to the interaction of the IMCs by 0.2 kcal $mol^{-1}$ less than the C—$H_{out}$···O hydrogen bond. This indicates that the second IMC arrangement, with four C—$H_{out}$···O hydrogen bonds, should be energetically favoured over the first one. This result is also consistent with that obtained by Gatti *et al.* (1994) applying QTAIM (Bader, 1990) to urea. However, in the more stable arrangement of the IMCs, *i.e.* when they are stabilized by four C—$H_{out}$···O contacts, the CL layer packing through N—$H_a$···O is disadvantageous because nearest the N—$H_a$ or C═O carboxamide groups of adjacent parallel IMCs are all pointing to one side of the CL layer. In contrast, in the less energetic arrangement of the IMCs, when four C—$H_{out}$···N contacts are built within the CL layer (*ab* layer), the nearest N—$H_a$ or C═O carboxamide groups of adjacent parallel IMCs are oriented in an alternating fashion at each side of the CL layer favouring their packing. The last IMC arrangement allows the diamide molecules to pack along the *c* axis *via* strong N—$H_a$···O hydrogen bonds, overcoming the small energy difference between the weak hydrogen bonds and promoting IMCs (within CL layer) being assembled in the less energetic arrangement. In this arrangement of the IMCs, cubyl C—$H_{out}$ groups should be pointing to carboxamide N atoms instead of O atoms. However, because C—H···O contacts are energetically more stable than C—H···N contacts, it might be inferred that the competition between these two weak contacts provokes a 'rotation' of the molecular chains of about 15°, around their chain axis. In this arrangement, two cubyl C—$H_{out}$ groups (oriented opposite along one of the cube diagonals) are pointing to the carboxamide O atoms of adjacent parallel IMCs, hence forming two C—$H_{out}$···O contacts instead of four C—$H_{out}$···N contacts. As a consequence of this, the carboxamide group plane is tilted out of the CL layer by an angle of $\theta_R \sim 75°$ (see Fig. 4*b*). As the CL layers are mainly connected by carboxamide interactions, through N—$H_a$···O hydrogen bonds, it affects the way these layers are assembled, causing them to be packed in a nonperpendicular direction. Assuming a carboxamide-group size of 5 Å, which is close to the carboxamide bond distance linked by N—$H_a$···O contacts, it is possible to express the parallel shift between CL layers ($\Delta$) in terms of $\theta_{IMC}$ (the tilt angle between the axis of the IMCs and the *c*-glide plane) and $\theta_R$ angles as $\Delta = 5\cos\theta_R\sin\theta_{IMC}$ (see part *a* in Fig. 9). The angle between the CL packing direction (which is coincident with the *c* axis) and the CL layer is the $\beta$ angle of the unit cell and can be calculated as $\cos\beta = -\Delta/5$, see Fig. 9(*b*), therefore $\cos\beta = -\cos\theta_R\sin\theta_{IMC}$. From the crystallographic data, $\theta_{IMC} = 43.85\ (1)°$, and the obtained value is $\beta = 100.5°$, which are very close to the observed value of 101.54° (Kuduva *et al.*, 2001). This provides evidence that weak intermolecular contacts acting within CL layers, in spite being much weaker than those established by carboxamide groups, might influence carboxamide orientation and therefore affect the molecular packing.

## 7. Conclusion

The effect of strong intermolecular N—$H_x$···O contacts established by carboxamide groups on the 3D ordering of molecules of *trans*-cyclohexane-1,4-dicarboxamide (**1**) and cubane-1,4-dicarboxamide (**2**) were analyzed in the context of their co-existence with weak intermolecular C—$H_y$···O contacts. As expected, experimental and theoretical results support the fact that strong intermolecular N—$H_x$···O inter-

actions determine the main characteristics of the molecular packing. Namely, they build infinite molecular chains through N—$H_s$···O contacts and these chains are packed by means of N—$H_a$···O contacts. In the crystalline state, the distribution of the electron charge density around the carbonyl O atom allows it to act as an electron donor not only in two strong N—$H_x$···O hydrogen bonds, of $n$(O)→$\sigma^*$($H_x$—N) type, but also in three weak C—$H_y$···O hydrogen bonds. One of the latter hydrogen bonds can be described as an $n$(O)→$\sigma^*$($H_{in}$—C) interaction, while the others can be described as $\pi$(C═O)→$\sigma^*$($H_{out}$—C) interactions. In addition, depending on whether these interactions involve molecular fragments with electronic charge delocalization, they contribute unevenly to co-operative effects, being capable of producing destabilizing effects, as in the case of the weak C—$H_{out}$···O contacts in **1**. However, in spite of this, as observed in **1** and **2**, weak intermolecular C—$H_y$···O hydrogen bonds are able to alter the approach of IMCs to form parallel layers and therefore affecting the carboxamide plane tilt with respect to the CL layer. As a result, due to the fact that the CL layers are mainly connected by N—$H_a$···O hydrogen bonds, differences in the carboxamide tilt cause **1** and **2** to be packed in different manners. Thus, it could be concluded that in **1** the $4_3$-fold screw axis is a consequence not only of the residue size but also of the residue morphology, which ultimately determines the arrangement of the C—H bonds with respect to the carboxamide-group plane.

## Acknowledgements

ACF, RMR, GP and GAE are research fellows of CONICET.

## Funding information

Funding for this research was provided by: Universidad Nacional de La Plata (award No. X-709); Consejo Nacional de Investigaciones Científicas y Técnicas (award No. PIP 0651); SNRX (award No. AC7).

## References

Agilent (2014). *CrysAlis PRO*. Agilent Technologies Ltd, Yarnton, Oxfordshire, England.
Bader, R. F. W. (1990). In *Atoms in Molecules: A Quantum Theory*. Oxford: Clarendon Press and Oxford Science Publications.
Barón, M., De Zenobi, E. L. & Davidson, M. (1975). *J. Mol. Struct.* **24**, 432–438.
Berkovitch-Yellin, Z. & Leiserowitz, L. (1980). *J. Am. Chem. Soc.* **102**, 7677–7690.
Biegler-König, F. & Schönbohm, J. (2002). *J. Comput. Chem.* **23**, 1489–1494.
Boys, S. F. & Bernardi, F. (1970). *Mol. Phys.* **19**, 553–566.
Cobbledick, R. E. & Small, R. W. H. (1972). *Acta Cryst.* B**28**, 2893–2896.
Desiraju, G. R. (1995). *Angew. Chem. Int. Ed. Engl.* **34**, 2311–2327.
Dovesi, R., Orlando, R., Erba, A., Zicovich-Wilson, C. M., Civalleri, B., Casassa, S., Maschio, L., Ferrabone, M., De La Pierre, M., D'Arco, P., Noel, Y., Causa, M., Rerat, M. & Kirtman, B. (2014). *Int. J. Quantum Chem.* **114**, 1287–1317.
Echeverría, G. A., Barón, M. & Punte, G. M. (2000). *Struct. Chem.* **11**, 35–40.
Echeverría, G. A., Goeta, A., Barón, M. & Punte, G. M. (2003). *Acta Cryst.* E**59**, o959–o961.
Echeverría, G. A., Punte, G. M., Rivero, B. E. & Barón, M. (1995*a*). *Acta Cryst.* C**51**, 1020–1023.
Echeverría, G. A., Punte, G. M., Rivero, B. E. & Barón, M. (1995*b*). *Acta Cryst.* C**51**, 1023–1026.
Farrugia, L. J. (1997). *J. Appl. Cryst.* **30**, 565.
Farrugia, L. J. (2012). *J. Appl. Cryst.* **45**, 849–854.
Frisch, M. J., *et al.* (2004). *GAUSSIAN03*. Gaussian Inc., Wallingford, CT, USA. http://www.gaussian.com.
Gatti, C. & Casassa, S. (2014). *TOPOND14 User's Manual*. CNR–ISTM Milano, Milano, Italy. http://www.crystal.unito.it/topond/topond.pdf.
Gatti, C., Saunders, V. R. & Roetti, C. (1994). *J. Chem. Phys.* **101**, 10686–10696.
Gilli, G., Bellucci, F., Ferretti, V. & Bertolasi, V. (1989). *J. Am. Chem. Soc.* **111**, 1023–1028.
Groom, C. R., Bruno, I. J., Lightfoot, M. P. & Ward, S. C. (2016). *Acta Cryst.* B**72**, 171–179.
Hongwei, T., Wenwen, Q., Guangju, C. & Ruozhuang, L. (2005). *J. Phys. Chem. A*, **109**, 6303–6308.
Jensen, F. (2007). In *Introduction to Computational Chemistry*, 2nd ed. London: John Wiley & Sons Ltd.
Kuduva, S. S., Bläser, D., Boese, R. & Desiraju, G. R. (2001). *J. Org. Chem.* **66**, 1621–1626.
Leiserowitz, L. (1976). *Acta Cryst.* B**32**, 775–802.
Leiserowitz, L. & Hagler, A. T. (1983). *Proc. R. Soc. London Ser. A*, **388**, 133–175.
Leiserowitz, L. & Schmidt, G. M. J. (1969). *J. Chem. Soc. A*, pp. 2372–2382.
Lin-Vien, D., Colthup, N. B., Fateley, W. G. & Grasselli, J. G. (1991). In *The Handbook of Infrared and Raman Characteristic Frequencies of Organic Molecules*. London: Academic Press Ltd.
Macrae, C. F., Bruno, I. J., Chisholm, J. A., Edgington, P. R., McCabe, P., Pidcock, E., Rodriguez-Monge, L., Taylor, R., van de Streek, J. & Wood, P. A. (2008). *J. Appl. Cryst.* **41**, 466–470.
Nardelli, M. (1995). *J. Appl. Cryst.* **28**, 659.
Parsons, S., Flack, H. D. & Wagner, T. (2013). *Acta Cryst.* B**69**, 249–259.
Reed, A. E. & Weinhold, F. (1986). *J. Chem. Phys.* **84**, 5687–5705.
Scott, A. P. & Radom, L. (1996). *J. Phys. Chem.* **100**, 16502–16513.
Sheldrick, G. M. (2015*a*). *Acta Cryst.* A**71**, 3–8.
Sheldrick, G. M. (2015*b*). *Acta Cryst.* C**71**, 3–8.
Simon, S., Duran, M. & Dannenberg, J. J. (1996). *J. Chem. Phys.* **105**, 11024–11031.
Spek, A. L. (2009). *Acta Cryst.* D**65**, 148–155.
Takamizawa, S. & Miyamoto, Y. (2014). *Angew. Chem. Int. Ed.* **53**, 6970–6973.
Van der Waals, J. D. (1873). Doctoral Dissertation, Leiden University, The Netherlands.
Zipp, C. F., Fernandes, M. A., Michael, J. P. & Winks, S. (2009). *Acta Cryst.* C**65**, o553–o554.

# supporting information

*Acta Cryst.* (2018). C**74** [https://doi.org/10.1107/S2053229618011750]

## Role of weak C—H···O and strong N—H···O intermolecular interactions on the high-symmetry molecular packing of *trans*-cyclohexane-1,4-dicarboxamide

**Fernando García-Reyes, Adolfo C. Fantoni, Máximo Barón, Rosana M. Romano, Graciela M. Punte and Gustavo A. Echeverría**

### Computing details

Data collection: *CrysAlis PRO* (Agilent, 2014); cell refinement: *CrysAlis PRO* (Agilent, 2014); data reduction: *CrysAlis PRO* (Agilent, 2014); program(s) used to solve structure: SHELXT (Sheldrick, 2015a); program(s) used to refine structure: *SHELXL2014* (Sheldrick, 2015b); molecular graphics: *ORTEP-3 for Windows* (Farrugia, 1997) and *Mercury* (Macrae *et al.*, 2008); software used to prepare material for publication: *PLATON* (Spek, 2009) and *PARST* (Nardelli, 1995) within *WinGX* (Farrugia, 2012).

### *trans*-Cyclohexane-1,4-dicarboxamide

*Crystal data*

$C_8H_{14}N_2O_2$
$M_r$ = 170.21
Tetragonal, $P4_32_12$
Hall symbol: P 4nw 2abw
$a$ = 6.9584 (2) Å
$c$ = 18.8979 (6) Å
$V$ = 915.02 (6) Å$^3$
$Z$ = 4
$F(000)$ = 368
$D_x$ = 1.236 Mg m$^{-3}$
Cu $K\alpha$ radiation, $\lambda$ = 1.54184 Å
Cell parameters from 854 reflections
$\theta$ = 4.7–69.5°
$\mu$ = 0.74 mm$^{-1}$
$T$ = 293 K
Frag, colourless
0.25 × 0.12 × 0.12 mm

*Data collection*

Agilent Xcalibur Eos Gemini diffractometer
Radiation source: Enhance (Cu) X-ray Source
Graphite monochromator
Detector resolution: 16.0604 pixels mm$^{-1}$
$\omega$ scans
Absorption correction: multi-scan (CrysAlis PRO; Agilent, 2014)
$T_{min}$ = 0.893, $T_{max}$ = 1
1745 measured reflections
890 independent reflections
837 reflections with $I > 2\sigma(I)$
$R_{int}$ = 0.014
$\theta_{max}$ = 72.0°, $\theta_{min}$ = 6.8°
$h$ = −8→8
$k$ = −6→7
$l$ = −11→23

*Refinement*

Refinement on $F^2$
Least-squares matrix: full
$R[F^2 > 2\sigma(F^2)]$ = 0.044
$wR(F^2)$ = 0.130
$S$ = 1.07
890 reflections
68 parameters
0 restraints
Hydrogen site location: difference Fourier map
Only H-atom displacement parameters refined
$w = 1/[\sigma^2(F_o^2) + (0.075P)^2 + 0.1598P]$ where $P = (F_o^2 + 2F_c^2)/3$

$(\Delta/\sigma)_{max} < 0.001$
$\Delta\rho_{max} = 0.23$ e Å$^{-3}$
$\Delta\rho_{min} = -0.13$ e Å$^{-3}$

Absolute structure: Flack *x* determined using 278 quotients [(I+)-(I-)]/[(I+)+(I-)] (Parsons *et al.*, 2013)
Absolute structure parameter: −0.1 (3)

*Special details*

**Geometry**. All e.s.d.'s (except the e.s.d. in the dihedral angle between two l.s. planes) are estimated using the full covariance matrix. The cell e.s.d.'s are taken into account individually in the estimation of e.s.d.'s in distances, angles and torsion angles; correlations between e.s.d.'s in cell parameters are only used when they are defined by crystal symmetry. An approximate (isotropic) treatment of cell e.s.d.'s is used for estimating e.s.d.'s involving l.s. planes.

**Refinement**. The measurements were performed on a Rigaku Oxford Diffraction EOS CCD diffractometer with graphite-monochromated Cu *Kα* ($\lambda$ = 1.54184 Å) radiation. X-ray diffraction intensities were collected ($\omega$ scans with $\theta$ and $\kappa$ offsets), integrated and scaled with *CrysAlis PRO* (Agilent, 2014) suite of programs. The unit-cell parameters were obtained by least-squares refinement (based on the angular settings for all collected reflections with intensities larger than seven times the standard deviation of measurement errors) using *CrysAlis PRO*. Data were corrected empirically for absorption employing the multi-scan method implemented in *CrysAlis PRO*. The molecular structure was solved by direct methods with *SHELXS* and the molecular model refined by full-matrix least-squares procedure with *SHELXL*, both codes belong to the *SHELX* suite of programs (2008). After non-hydrogen atoms were anisotropically refined, hydrogen atoms were localized from Fourier difference maps and refined riding on bound atoms. *ORTEP-3 for Windows* (Farrugia, 1997) and Mercury (Macrae *et al.*, 2006) programs were used for structure analysis and to prepare material for publication. Details of data collection and structure refinement are summarized in Table 1. *PLATON* (Spek, 2009) and *PARST* (Nardelli, 1995) programs were used within *WinGX* (Farrugia, 2012) to prepare tables for publication.

*Fractional atomic coordinates and isotropic or equivalent isotropic displacement parameters (Å²)*

| | *x* | *y* | *z* | $U_{iso}$*/$U_{eq}$ |
|---|---|---|---|---|
| O5 | 0.3771 (3) | 1.0600 (3) | 0.54566 (9) | 0.0602 (6) |
| N6 | 0.3328 (4) | 1.0717 (4) | 0.42891 (11) | 0.0549 (7) |
| H62 | 0.367 (5) | 1.033 (6) | 0.3894 (17) | 0.067 (10)* |
| H61 | 0.245 (6) | 1.159 (6) | 0.4352 (17) | 0.070 (10)* |
| C4 | 0.4181 (3) | 1.0038 (3) | 0.48545 (11) | 0.0425 (6) |
| C1 | 0.5696 (4) | 0.8512 (4) | 0.47394 (12) | 0.0458 (6) |
| H11 | 0.5774 | 0.8366 | 0.4274 | 0.051 (8)* |
| C3 | 0.7604 (4) | 0.9142 (4) | 0.5055 (2) | 0.0696 (9) |
| H31 | 0.7398 | 0.9341 | 0.5572 | 0.072 (10)* |
| H32 | 0.7948 | 1.0401 | 0.4778 | 0.135 (18)* |
| C2 | 0.5077 (4) | 0.6614 (4) | 0.5047 (2) | 0.0694 (10) |
| H21 | 0.4976 | 0.6845 | 0.5572 | 0.073 (10)* |
| H22 | 0.3798 | 0.6212 | 0.481 | 0.084 (12)* |

*Atomic displacement parameters (Å²)*

| | $U^{11}$ | $U^{22}$ | $U^{33}$ | $U^{12}$ | $U^{13}$ | $U^{23}$ |
|---|---|---|---|---|---|---|
| O5 | 0.0700 (13) | 0.0727 (13) | 0.0379 (8) | 0.0316 (10) | −0.0028 (8) | −0.0087 (8) |
| N6 | 0.0645 (14) | 0.0621 (14) | 0.0381 (10) | 0.0287 (12) | −0.0010 (9) | −0.0008 (9) |
| C4 | 0.0455 (12) | 0.0434 (12) | 0.0387 (11) | 0.0097 (9) | −0.0002 (9) | −0.0026 (9) |
| C1 | 0.0520 (14) | 0.0484 (13) | 0.0371 (10) | 0.0170 (11) | 0.0020 (10) | −0.0034 (9) |
| C3 | 0.0443 (14) | 0.0422 (14) | 0.122 (3) | 0.0028 (12) | 0.0018 (17) | −0.0071 (16) |
| C2 | 0.0384 (13) | 0.0478 (16) | 0.122 (3) | 0.0028 (12) | 0.0023 (17) | −0.0006 (17) |

*Geometric parameters (Å, º)*

| | | | |
|---|---|---|---|
| O5—C4 | 1.237 (3) | C1—H11 | 0.8876 |
| N6—C4 | 1.311 (3) | C3—C3$^{i}$ | 1.528 (6) |
| N6—H62 | 0.83 (3) | C3—H31 | 0.9969 |
| N6—H61 | 0.87 (4) | C3—H32 | 1.0476 |
| C4—C1 | 1.511 (3) | C2—C2$^{i}$ | 1.523 (5) |
| C1—C2 | 1.506 (4) | C2—H21 | 1.0078 |
| C1—C3 | 1.520 (4) | C2—H22 | 1.0349 |
| | | | |
| C4—N6—H62 | 119 (2) | C1—C3—C3$^{i}$ | 110.9 (2) |
| C4—N6—H61 | 117 (2) | C1—C3—H31 | 107.4 |
| H62—N6—H61 | 123 (3) | C3$^{i}$—C3—H31 | 109.3 |
| O5—C4—N6 | 122.1 (2) | C1—C3—H32 | 104.2 |
| O5—C4—C1 | 121.1 (2) | C3$^{i}$—C3—H32 | 111 |
| N6—C4—C1 | 116.9 (2) | H31—C3—H32 | 113.9 |
| C2—C1—C4 | 111.2 (2) | C1—C2—C2$^{i}$ | 111.7 (2) |
| C2—C1—C3 | 110.6 (2) | C1—C2—H21 | 105.1 |
| C4—C1—C3 | 110.5 (2) | C2$^{i}$—C2—H21 | 106 |
| C2—C1—H11 | 107.5 | C1—C2—H22 | 108.4 |
| C4—C1—H11 | 105.4 | C2$^{i}$—C2—H22 | 111.3 |
| C3—C1—H11 | 111.6 | H21—C2—H22 | 114.2 |
| | | | |
| O5—C4—C1—C2 | 65.6 (4) | C2—C1—C3—C3$^{i}$ | 56.2 (4) |
| N6—C4—C1—C2 | −114.0 (3) | C4—C1—C3—C3$^{i}$ | 179.6 (3) |
| O5—C4—C1—C3 | −57.5 (4) | C4—C1—C2—C2$^{i}$ | −178.4 (3) |
| N6—C4—C1—C3 | 122.8 (3) | C3—C1—C2—C2$^{i}$ | −55.3 (4) |

Symmetry code: (i) *y*, *x*, −*z*+1.

*Hydrogen-bond geometry (Å, º)*

| *D*—H···*A* | *D*—H | H···*A* | *D*···*A* | *D*—H···*A* |
|---|---|---|---|---|
| N6—H62···O5$^{ii}$ | 0.83 (3) | 2.14 (4) | 2.955 (3) | 169 (4) |
| N6—H61···O5$^{iii}$ | 0.87 (4) | 2.02 (4) | 2.889 (3) | 175 (4) |
| N6—H62···O5$^{ii}$ | 0.83 (3) | 2.14 (4) | 2.955 (3) | 169 (4) |
| N6—H61···O5$^{iii}$ | 0.87 (4) | 2.02 (4) | 2.889 (3) | 175 (4) |
| C1—H11···O5$^{ii}$ | 0.89 | 2.68 | 3.492 (3) | 152.5 |
| C2—H22···O5$^{iv}$ | 1.03 | 2.84 | 3.811 (4) | 155.6 |
| C3—H32···O5$^{v}$ | 1.05 | 3.02 | 3.956 (4) | 149.7 |

Symmetry codes: (ii) −*y*+3/2, *x*+1/2, *z*−1/4; (iii) *y*−1, *x*+1, −*z*+1; (iv) *y*−1, *x*, −*z*+1; (v) *y*, *x*+1, −*z*+1.

*Topological analysis of selected contacts calculated at PBE/6-31G** theory level for clusters **I** and **II**[a]*

| Contact | Comp | $\rho$ | \nabla$^2$ (e A$^{-3}$) | $\lambda_3$ (e A$^{-3}$) | $G$ (kcal mol$^{-1}$) | $V$ (kcal mol$^{-1}$) | $H$ (kcal mol$^{-1}$) |
|---|---|---|---|---|---|---|---|
| N—H$_s$···O | **1** | 0.2247 | 2.2884 | 4.5124 | 15.5 | -16.1 | -0.6 |
| | **2** | 0.2314 | 2.4308 | 4.7490 | 16.3 | -16.7 | -0.4 |
| N—H$_a$···O | **1** | 0.1566 | 1.7486 | 3.1217 | 11.6 | -11.9 | -0.3 |
| | **2** | 0.1718 | 1.8356 | 3.3832 | 12.4 | -12.9 | -0.5 |

| | | | | | | | |
|---|---|---|---|---|---|---|---|
| C—$H_{in}$···O | **1** | 0.0469 | 0.5597 | 0.8408 | 3.2 | -2.8 | 0.4 |
| | **2** | 0.0803 | 0.8597 | 1.4336 | 5.6 | -5.5 | 0.1 |
| C—$H_{out}$···O | **1** | 0.0453 | 0.5792 | 0.8289 | 3.3 | -2.7 | 0.6 |
| | **2** | 0.0455 | 0.5647 | 0.8433 | 3.2 | -2.7 | 0.5 |

(*a*) $\rho$(r) electron density, its Laplacian, \nable$^2\rho$(r), positive principal curvature, $\lambda_3$, G(r) kinetic, V(r) potential and H(r) total energy densities evaluated at the corresponding (3,-1) critical points.